Study of Microstructure of Low-Temperature Plasma-Nitrided AISI 304 Stainless Steel

XIAOLEI XU, LIANG WANG, ZHIWEI YU, JIANBING QIANG, and ZUKUN HEI

The microstructure of the low-temperature plasma-nitrided layer on AISI 304 austenitic stainless steel was studied by transmission electron microscopy (TEM). The results show that the surface of the layer consists of a supersaturated solid solution (γ'_N) based on the γ'-Fe_4N phase whose electron diffraction pattern (EDP) has a strong diffuse scattering effect resulting from supersaturating nitrogen (above 20 at. pct) and ⟨110⟩ streaks arising from matrix elastic strain due to the formation of paired or clustered Cr-N. The latter is due to the N above the 20 at. pct γ'-Fe_4N–phase value and leads to a lattice parameter that is greater than that of the γ'-Fe_4N phase. The subsurface of the layer is composed of a supersaturated solid solution based on γ-austenite, which is an expanded austenite, γ_N. Its morphology shows the basketweave or "tweedlike" contrast consisting of so-called stacking fault precipitates having twin relationships with the matrix whose EDP shows diffuse scattering streaks with certain directions. The ε martensite transformation was observed in the subsurface of the layer. The increase in stacking faults compared with the original stainless steel and formation of ε martensite in the subsurface of the layer indicate that nitrogen lowers the stacking fault energy of austenite.

I. INTRODUCTION

STAINLESS steel is widely used in chemical, food, and other industries due to its corrosion-resistance properties. However, because of its low hardness or poor wear-resistance properties, its application is greatly limited. Scientists have paid much attention to the surface modification of stainless steel. Many attempts have been made to increase the surface hardness of this material using such techniques as plasma source ion implantation (PSII), plasma ion implantation (PII), and plasma nitriding[1–3]. An increase in surface hardness is often accompanied by a decrease in corrosion properties due to precipitating CrN, especially in the traditional plasma nitriding used widely in industry production. Zhang and Bell[4] reported for the first time that the S-phase formation on the surface by reducing treatment temperature of the plasma nitriding can provide both wear resistance and corrosion resistance. This S-phase has become known as γ_N in later research because the basic fcc structure (γ-austenite) is retained. However, despite many investigations[5–8] the exact nature of the microstructural changes responsible for this improvement is not very well understood. Using most techniques, the lattice parameter of the so-called γ_N is greater than that of the γ'-Fe_4N ($a = 0.379$, nm) and its nitrogen content more than 20 at. pct.[7,8] It is uncertain whether the supersaturated solid solution is based on the γ'-Fe_4N or γ-austenite or on both. In other words, there would be two kinds of supersaturated solid solution respectively based on either γ'-Fe_4N or γ-austenite. However, there is a difference between γ'-Fe_4N and γ-austenite in crystal structure. The former has nitrogen atoms occupying octahedral interstitial sites of cube center in a fully ordered manner, and the latter has nitrogen atoms randomly distributed throughout all interstitial octahedral sites. In this article, we will address this issue using transmission electron microscopy (TEM). In order to understand the present work more easily, it is necessary to pronouncedly define the phases dealt with in the article as follows.

γ-austenite—the solid solution of nitrogen in γ-Fe (fcc),[9] in which nitrogen atoms occupy the octahedral holes of fcc lattice in a disordered manner; γ'-Fe_4N—the ordered solid solution, in which the metal atoms arrangement is fcc, but the nitrogen atoms occupy one-quarter of the number of octahedral holes in a fully ordered manner;[9] S or γ_N—the supersaturated solid solution of nitrogen in γ austenite or the nitrogen expanded austenite, in which nitrogen atoms occupy the octahedral holes in a disordered manner;[4] γ'_N—the supersaturated solid solution of nitrogen in γ'-Fe_4N, which is defined by the present work; ε—martensite: a hcp phase with ideal *c*/*a* radio, nitrogen-induced martensite, which is similar to the martensite strain induced[10] or hydrogen induced;[11] and CrN—chromium nitride (fcc).

II. EXPERIMENT METHODS

The AISI 304 stainless steels annealed were used in this study. The composition of the material was (in wt pct) C0.15, Mn2.0, Si1.0, Ni8, Cr18, and Fe balance. Plasma nitriding was carried in an LD-10 kW commercial plasma-nitriding furnace equipped with an electron-beam source of 50 A. The activity and ionization ratio of the nitriding gas can be raised by electron bombardment of the gas. A high efficiency plasma nitriding can be achieved at the low temperature. A schematic of the nitriding system used in this work is shown in Figure 1. The samples were plasma nitrided for 2 hours at 400 °C to about 420 °C in a $4N_2$: H_2 atmosphere at a total pressure of 0.3 Pa. The samples for TEM were prepared by grinding and mechanical polishing from the untreated side to 40 μm, followed by ion thinning from the untreated side to make the thin foil for the layer surface, and from layer-surface side to make the thin foils for the subsurface 8 to

XIAOLEI XU, LIANG WANG, and ZHIWEI YU, Associate Professors, JIANBING QIANG, Master, and ZUKUN HEI, Professor and Director, are with the Institute of Metal and Technology, Dalian Maritime University, Dalian 116024, People's Republic of China.

Manuscript submitted December 11, 1998.

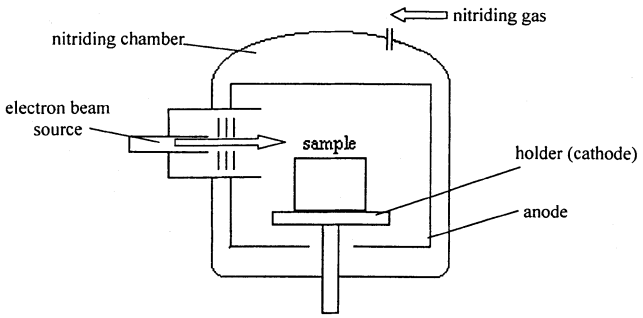

Fig. 1—Plasma nitriding system.

about 9 μm below surface and matrix. The TEM observations were made with a Hitachi 800 transmission electron microscope at an acceleration voltage of 175 kV.

The phases present in the plasma-nitrided layer were determined by glancing angle X-ray diffraction (XRD) on a Rigaku D/max-IIIA diffractometer. The radiation used was Cu $K\alpha$ ($\lambda = 0.1542$ nm) at incident angles of 10 deg.

III. RESULTS AND DISCUSSIONS

A. *XRD Results*

X-ray difraction patterns of the plasma-nitrided and untreated samples are shown in Figure 2. It is demonstrated that the untreated sample is single-phase γ-austenite, and its peaks are sharp, which is typical of annealed materials. For the plasma-nitrided sample, all peaks were shifted to the lower angles and were broadened considerably. Peaks appear at $2\theta = 39.55$ deg, 45.45 deg, and 67.65 deg corresponding to plane spacings of $d = 0.228$ nm, $d = 0.199$ nm, and $d = 0.138$ nm, respectively. The shift is associated with the expanded fcc phase caused by the nitrogen remaining in solid solution in the fcc lattice. The broadening for peaks results from the inhomogeneous stress produced by supersaturating nitrogen and nonuniform nitrogen content over the depth range of XRD.[7] The XRD results show that the nitrided layer is mainly composed of supersaturated solid solutions with an expanded fcc structure, and the lattice parameter of the supersaturated lattice determined by XRD surpasses that of the γ'-Fe_4N phase. Because the intensity of X-ray is much lower than the intensity of electron diffraction and is more restricted by atomic number than the latter, the ordering diffraction peaks related to the arrangement role of the light atoms (nitrogen atoms) in the lattice are not detectable by XRD. It is difficult to determine whether the supersaturated solid solution is based on γ'-Fe_4N or γ-austenite by XRD or whether there are two kinds of solid solution based on the different phases at different depths from the surface.

B. *TEM Results*

A scanning electron microscopy (SEM) morphology giving the entire nitriding zone is shown in Figure 3 (observed in a JEOL* 35 CF scanning microscope). Thickness of the nitrided layer is about 10 μm. The TEM specimens were located on the layer surface and in the subsurface at 8 to about 9 μm below surface (marked A and B).

*JEOL is a trademark of Japan Electron Optics Ltd., Tokyo.

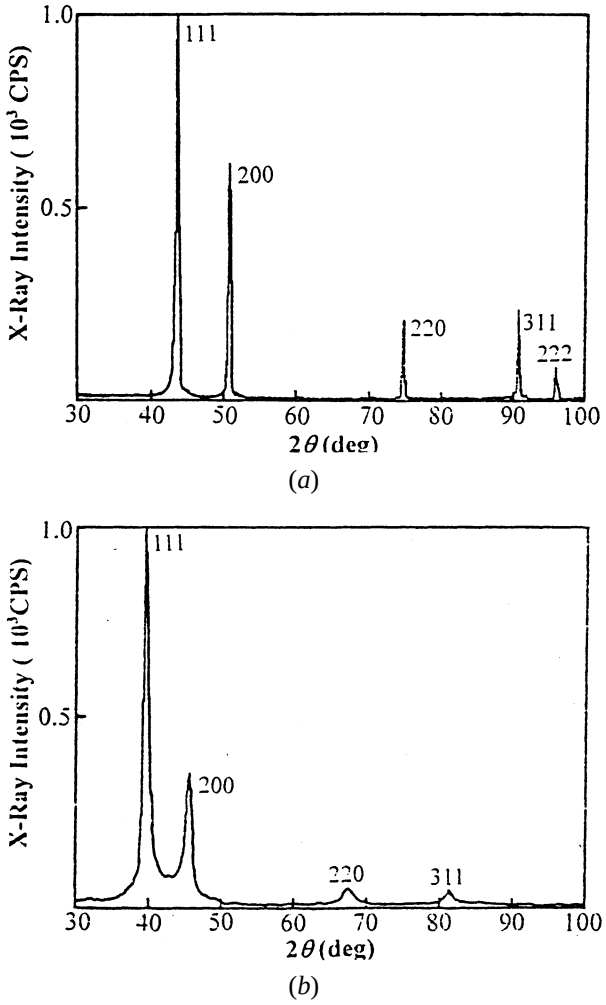

Fig. 2—X-ray diffraction patterns for untreated and plasma-nitrided 304 stainless steel: (*a*) untreated and (*b*) plasma nitrided.

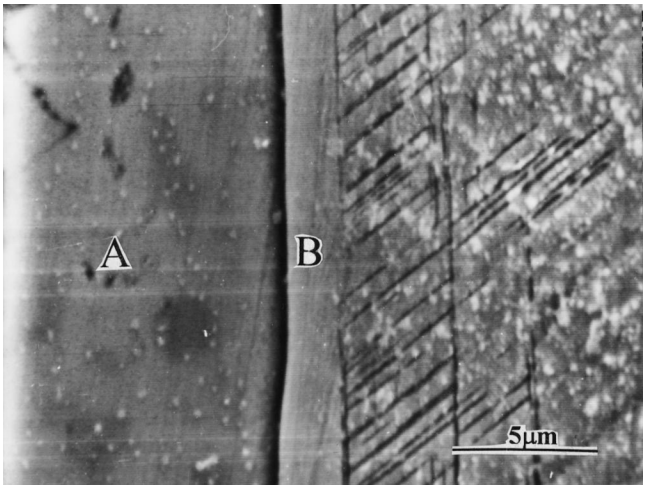

Fig. 3—SEM morphology of the nitriding layer for a 304 stainless steel etching solution: $CuSO_4 \cdot 5H_2O$ (20 g) + HCl (100 mL) + H_2SO_4 (5 mL) + H_2O (80 mL).

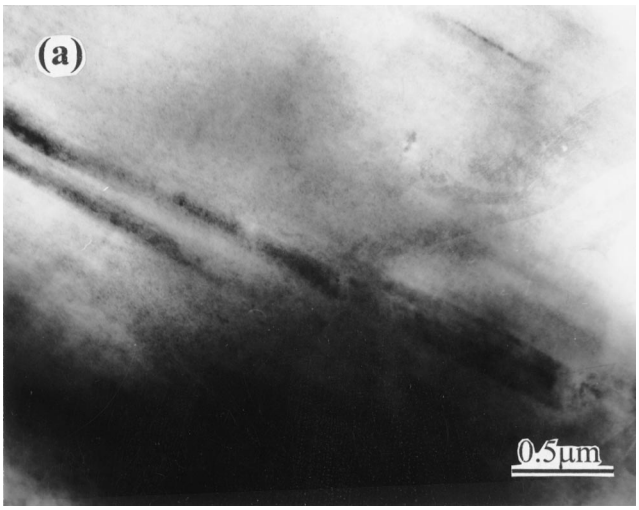

Fig. 4—Microstructure of the nitrided layer surface (γ'_N) and its electron diffraction pattern: (*a*) bright-field image and (*b*) EDP.

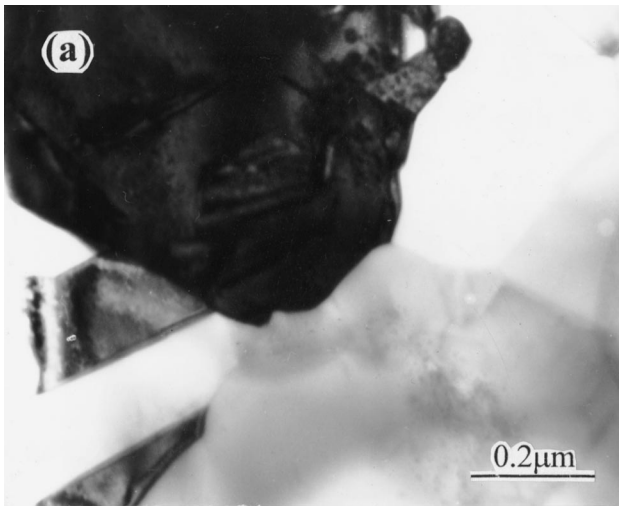

Fig. 5—Microstructure of pure γ'-Fe_4N and its electron diffraction pattern (pure iron plasma nitrided at 550 °C): (*a*) morphology and (*b*) EDP.

1. *Microstructure on the surface of the nitrided layer.*

The microstructure of the layer surface is shown in Figure 4(a). Its electron diffraction pattern (Figure 4(b)) indicates that it is an ordered fcc phase similar to the γ'-Fe_4N phase, but the lattice parameter is larger than that of γ'-Fe_4N. After determining accurately the camera constant ($L\lambda$) using the electron diffraction rings of Au, the lattice parameter of the fcc phase was determined from the EDP as 0.394 to about 0.400 nm, which is in good agreement with the results of XRD. More importantly, compared with the electron diffraction pattern of γ'-Fe_4N obtained by the usual plasma-nitriding technology, such as pure iron nitrided at 550 °C (Figure 5) or other ferrite steels,[12] in which there are clear superlattice reflections resulting from the nitrogen atoms at octahedral interstitials of cube center besides the fundamental reflections resulting from the Fe atoms at fcc lattice, the electron diffraction pattern in Figure 4(b) shows an obvious diffuse scattering effect in the form of the broadening of the fundamental reflections and the diffuse scattering streaks along ⟨100⟩. It is well known that solid solutions with short-range order usually exhibit diffuse intensity maxima in electron diffraction patterns.[13] It should be noted that the superlattice reflections in the EDP of Figure 4(b) are not as clear as the ones in Figure 5(b). It is suggested that the supersaturated solid solution with short-range order is based on γ'-Fe_4N, but supersaturating with nitrogen beyond 20 at. pct does not make the long-range order of γ'-Fe_4N change. It is well known that the stable γ'-Fe_4N has a very narrow nitrogen-concentration range (5.30 wt pct to about 5.75 wt pct), about 20 at. pct. The AISI 304 stainless steel contains a high concentration of Cr atoms and the bonding between Cr and N is greater than between Fe and N or Ni and N,[8] which is consistent with the formation trend of CrN at high temperatures. However, Cr atoms have lower diffusion ability at the low temperature so that pairs or clusters of the Cr and N could form without precipitation of the compound CrN. The Cr atoms occupy substitutively fcc lattice sites and combine with nitrogen atoms clustering at octahedral interstitials at the midpoints of cube edges of $\{001\}_{\gamma'\text{-}Fe_4N}$ to form Cr-N pairs or clusters. It is the presence of Cr atoms in the stainless steel that makes supersaturating nitrogen in γ'-Fe_4N possible. In fact, the image contrast for the supersaturated γ'-Fe_4N is quite different from the γ'-Fe_4N obtained by plasma-nitriding pure iron (Figure 5) or usual ferrite steels. From Figure 4(a), good diffraction contrast cannot be observed,

and no matter what the thickness of the foil is or the orientation of the grain observed is, good contrast could not be obtained. It seems that it has the characteristic of an amorphous phase contrast to some extent. The Cr-N pairs or clusters in the supersaturated solid solution is short-range ordering but long-range disordering due to the random site occupation of the Cr, which contributes to the poor diffraction contrast and diffuse scattering effect. The poor diffraction contrast and corresponding diffuse scattering effects observed and the lattice parameter greater than γ'-Fe_4N demonstrate that a metastable supersaturated solid solution has formed on the layer surface and is based on γ'-Fe_4N. We suggest this phase should be known as γ'_N to distinguish it from γ_N. Additionally, the electron diffraction pattern (Figure 4(b)) shows [110] and [$\bar{1}$10] streaks at the (020) and ($\bar{2}$00) reflections. Streaks can arise in diffraction patterns because of modification to the shape of reciprocal lattice points arising from either shape effects of crystal defects and precipitates or from the lattice strain associated with them, *i.e.*, elastic strain effects. Often the elastic distortion of the matrix resulting from a coherent misfitting produces diffuse scattering in reciprocal space in the direction of the distortion. It is difficult to separate streaks resulting from the elastic distortion of the matrix from the shape effects of the precipitates because they occur in the same direction. The pairs or clusters of Cr-N on {100} matrix planes can produce shape streaks in reciprocal space in ⟨100⟩. However the coherency strains are shear strains in ⟨110⟩* and produce streaks parallel to ⟨110⟩ in reciprocal space. The streaks resulting from the matrix elastic strain also demonstrate that the supersaturated solid solution (γ'_N) contains Cr-N clusters with short-range ordering, and these form on the layer surface.

2. *Microstructure in the subsurface of the nitrided layer*

The microstructure of the subsurface and its electron diffraction pattern are shown in Figure 6. The EDP indicates that it is an fcc phase, but the lattice parameter is greater than that of the γ-austenite, attaining 0.370 nm but less than that of γ'-Fe_4N. There are no superlattice reflections. This fcc phase should be considered to be γ_N phase, which is the supersaturated solid solution of nitrogen in γ-austenite. It should be noted that there are diffuse scattering streaks with certain directions in the EDP. The images exhibit a distinctive basketweave or "tweedlike" contrast consisting of two sets of striations. The inspection of the diffraction pattern reveals two components of diffuse scattering (at the fundamental reflections) normal to each set of striations. The diffuse directions should be interaction lines of the diffuse reciprocal plane and reciprocal plane photographed, or the striations of the basketweave should be the intersection line of the diffuse plane with the foil plane. By trace analysis, the directions of striations are just the intersection directions of {111} planes with the foil plane. In Figure 6, the intersection line for ($\bar{1}$11) with (11$\bar{2}$) is [312] and (1$\bar{1}$1) with (11$\bar{2}$) is [132], and the angle between [312] and [132] is 44.89 deg, which is identical with the angle between striations (indicated in Figure 6(a)). Although it is difficult to measure the length of the diffuse streaks, it is expected that the length is related to striation width, which is related to the thickness of the striations. The width for the striations in the image

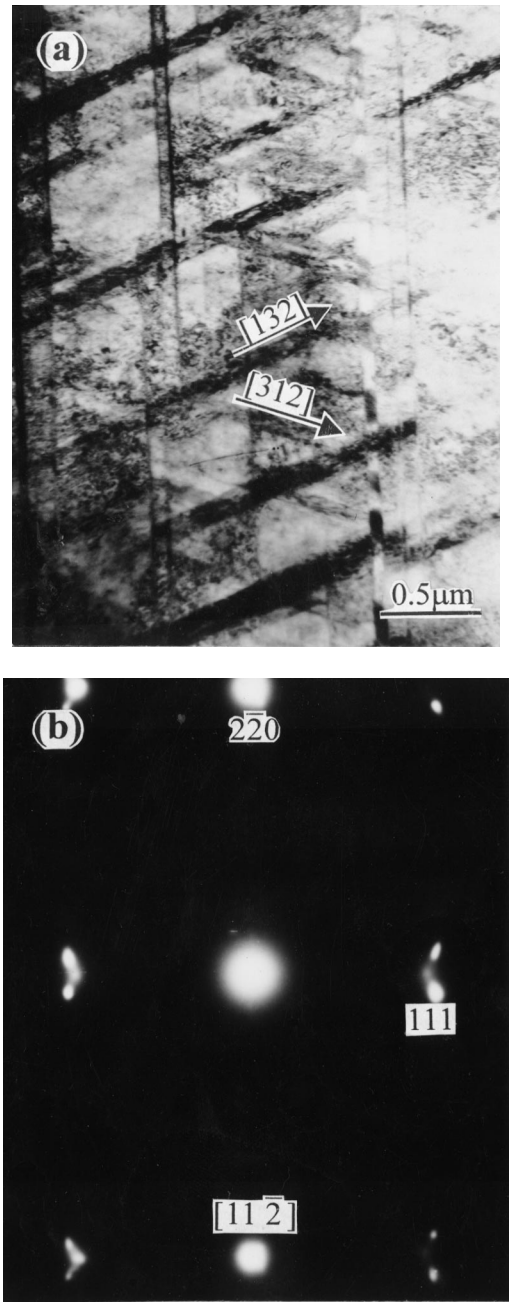

Fig. 6—Microstructure of the subsurface (γ_N) with striations of the stacking fault and electron diffraction pattern: (*a*) bright-field image and (*b*) EDP.

is related to the orientation between the {111} planes and the foil plane, and it is the real width only when the {111} planes are normal to the foil plane. When the {111} planes are not normal to the foil plane, the width in the image must be wider than the real width.

The described trace analysis and the corresponding microstructure and EDP demonstrate that stacking faults are prominent features in the γ_N layer. In other words, the so-called stacking fault precipitates form, whose morphology seems to exhibit the precipitation contrast, and two sets of striations seem to be the precipitates, but they are only stacking faults. By tilting the specimen, it has been found that stacking fault

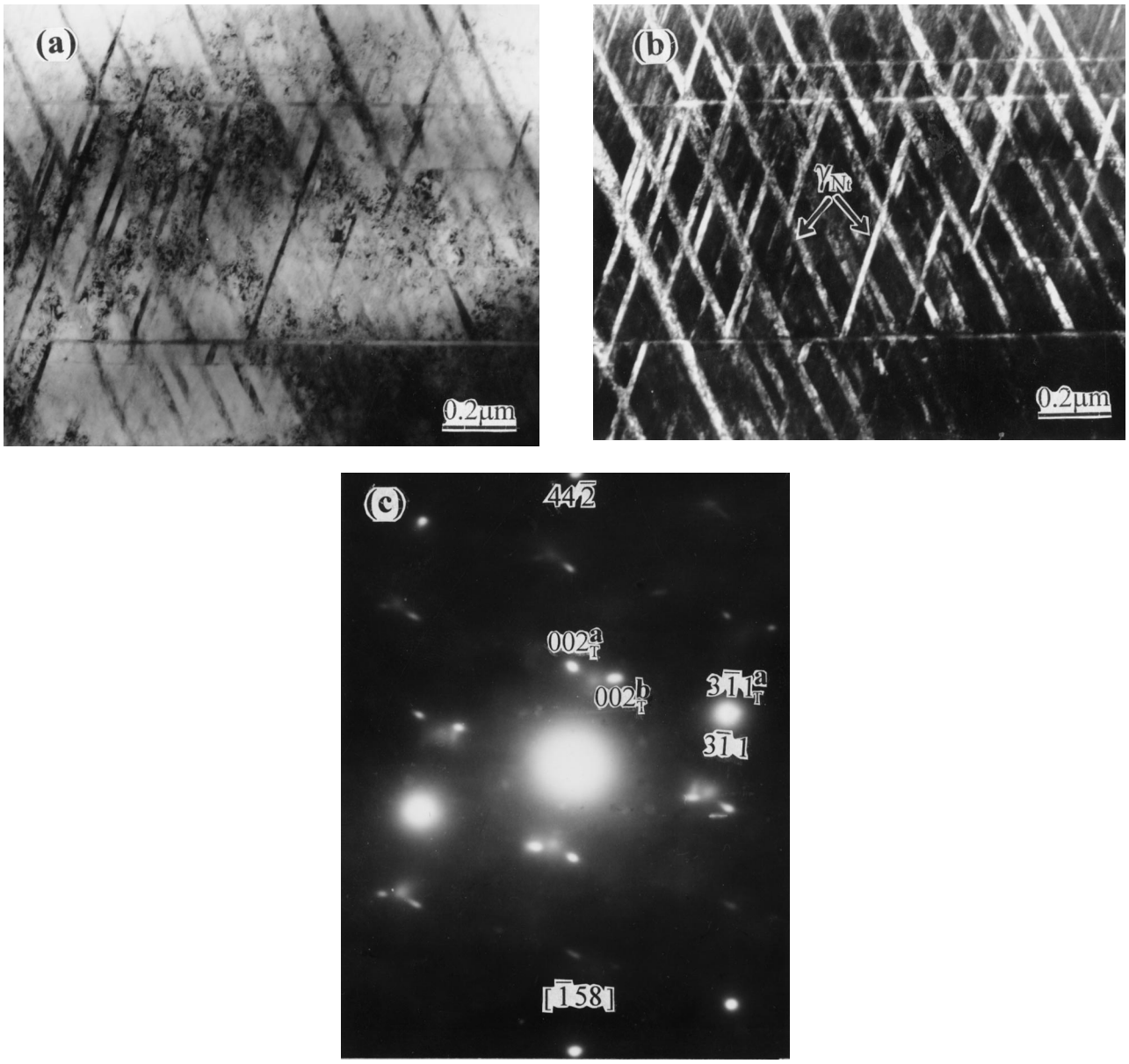

Fig. 7—Microstructure of the subsurface showing γ_N twin and its electron diffraction pattern: (*a*) bright-field image, (*b*) dark-field image ($g = 002_T$(A), $g = 002_T$(B)), and (*c*) EDP.

precipitate with two different directions are two variants of γ_N (shown by arrows), which have twin relationships with the γ_N matrix (Figure 7). The variants should be considered as the deformed twins induced by the stress resulting from supersaturating nitrogen. Stacking fault precipitates or deformed twins have a random stacking fault arrangement. It is interesting that ε martensite was observed in the subsurface layer (Figure 8), which is not randomly faulted fcc, such as stacking fault precipitates or deformed twins described previously, but a perfect hcp phase.[10] From Figure 8, the two ε variants (indicated by arrows) form on {111} γ_N whose morphology is similar to the stacking fault precipitate described previously. In fact, the striations of stacking faults would nucleate the ε phase. When the randomly faulted fcc develop into the regularly faulted fcc, an hcp phase with an ideal *c*/*a* ratio would form. In fact, the ε martensite would form by the glide of Shockley partial dislocations on each alternate matrix plane {111} in the lower stacking fault energy alloy. It is suggested that supersaturating nitrogen may lower the stacking fault energy to such a low value that the strain associated with nitrogen in solution causes the transformation to proceed by $\gamma_N \rightarrow \varepsilon$, which is similar to the marstensite transformation induced by hydrogen.[11] The orientation relationship between the γ_N and ε is identical with one in the strain-induced transformation and hydrogen induced.[10,11] All in all, the formation of the ε phase and observation of extensive stacking faults in nitrided material are good evidence that the nitrogen lowers the stacking fault energy of austenitic stainless steel.

3. *Microstructure of the matrix*

The microstructure of the matrix is shown in Figure 9. It is apparent that it is quite different from that of the γ_N phase.

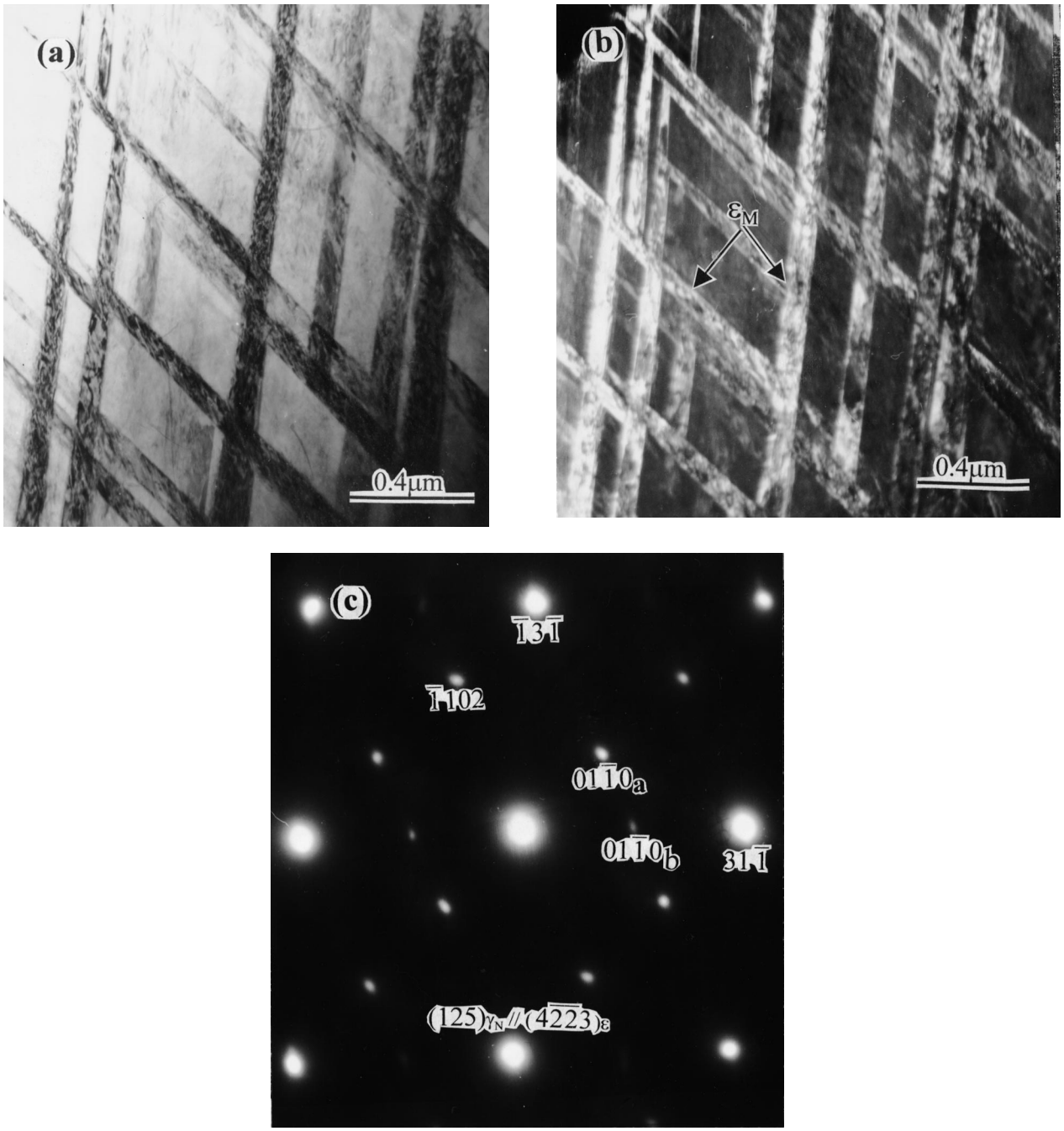

Fig. 8—Microstructure of the subsurface showing ε martensite and electron diffraction pattern: (*a*) bright-field image, (*b*) dark-field image ($g = 01\bar{1}0_a$, $g = 01\bar{1}0_b$), and (c) EDP.

It exhibits the characteristic of an annealed structure without stacking fault precipitates and formation of ε martensite.

IV. CONCLUSIONS

1. The surface of the nitrided layer consists of the supersaturated solid solution γ'-Fe_4N-type structure with additional short-range order Cr-N pairs or clusters γ'_N. Its electron diffraction pattern demonstrates strong diffuse scattering effects, and its lattice parameter is significantly greater than that of γ'-Fe_4N.
2. The subsurface of the nitrided layer consists of the supersaturated solid solution γ-austenite-type structure, which is an expanded austenite, γ_N. The microstructure shows basketweave or tweedlike morphology, which are striations of stacking faults or deformed twins and ε-martensite.
3. The observation of extensive stacking faults and formation of ε-martensite indicate that nitrogen in solid solution lowers the stacking fault energy of austenite in 304 stainless steel.

ACKNOWLEDGMENTS

This project was funded by the Liaoning Province Natural Science Foundation.

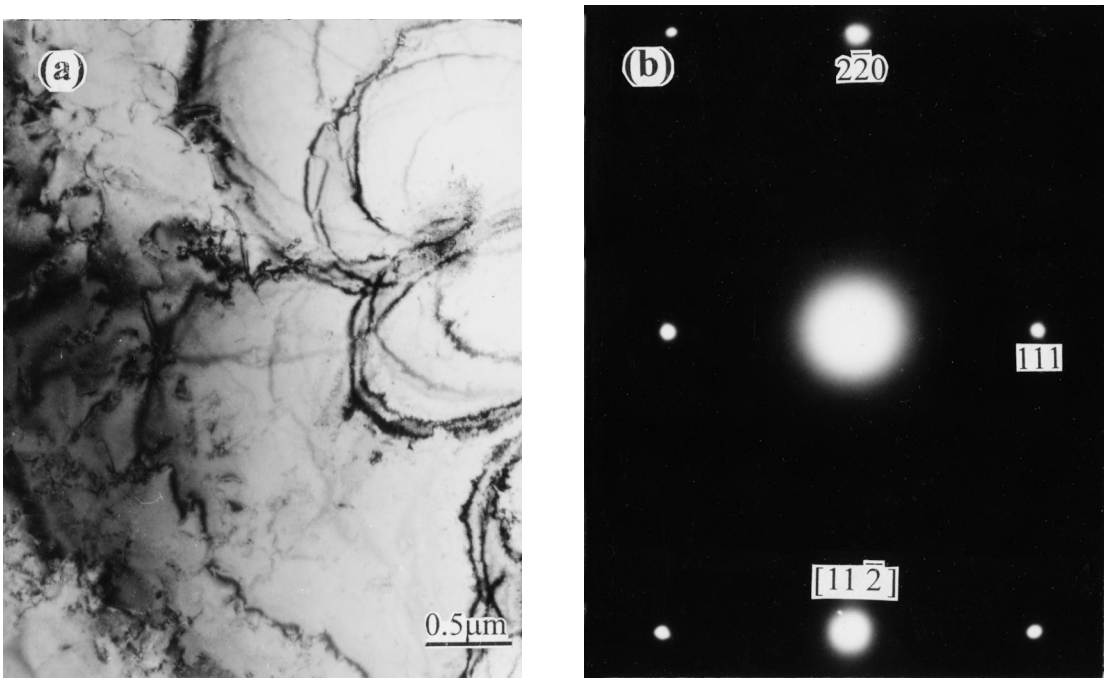

Fig. 9—Microstructure and electron diffraction pattern of matrix (a nitrided 304 stainless steel): (*a*) morphology and (*b*) EDP.

REFERENCES

1. X. Li, M. Samandi, D. Dunne, G. Collins, J. Tendys, K. Short, and R. Hutching: *Surf. Coat. Technol.*, 1996, vol. 85, pp. 28-36.
2. R.Wei, J.J. Vajo, J.N. Matossian, P.J. Wilbur, J.A. Davis and D.L. Williamson: *Surf. Coat. Technol.*, 1996, vol. 83, pp. 235-42.
3. D.L. Williamson, Li Wang, R. Wei, and P.J. Wilbur: *Mater. Lett.*, 1990, vol. 9, pp. 302-08.
4. Z.L. Zhang and T. Bell: *Sur. Eng.*, 1985, vol. 1, pp. 131-36.
5. Menthe, K.-T. Rie, J.W. Schultze, and S. Simson: *Surf. Coat. Technol.*, 1995, vols. 74–75, pp. 412-16
6. A. Saker, C. Leroy, H. Michel, and C. Frantz: *Mater. Sci. Eng.*, 1991, vol. 140, pp. 702-08.
7. Orhan Ozturk and D.L. Williamson: *J. Appl. Phys.*, 1995, vol. 77, pp. 3839-50.
8. D.L. Williamson, O. Ozturk, R. Wei, and P.J. Wilbur: *Surf. Coat. Technol.*, 1994, vol. 65, pp. 15-23.
9. D.H. Jack and K.H. Jack: *Mater. Sci. Eng.*, 1973, vol. 11, pp. 1-27.
10. Pat L. Mangonon, Jr. and Gareth Thomas: *Metall. Trans.* 1970, vol. 6, pp. 1577-86.
11. J.M. Rigsbee: *Metallography*, 1978, vol. 11, pp. 493-98.
12. Xiaolei Xu, Liang Wang, Zhiwei Yu, and Zukun Hei: *Metall. Trans. A*, 1996, vol. 27A, pp. 1347-52.
13. J.W. Edington: *Practical Electron Microscopy in Materials Science (Part II)*, The Macmillan Press Ltd., London, 1975.